AIAA JOURNAL
Vol. 47, No. 5, May 2009

Development of Homogeneous Water Condensation Models Using Molecular Dynamics

Zheng Li,* Jiaqiang Zhong,† Deborah A. Levin,‡ and Barbara J. Garrison§
Pennsylvania State University, University Park, Pennsylvania 16802

DOI: 10.2514/1.40360

A condensation phenomenon in free expansion plumes has been observed and studied in the past several decades. To model homogeneous condensation of small, polar molecules produced in the combustion products of chemical propellants, such as water, accurate microscopic cluster models need to be developed. In this work, the molecular dynamics method is used to develop a model of water cluster sizes, cluster–monomer collisions, and sticking probabilities necessary for the study of water homogeneous condensation in a plume expanding to low pressure, space conditions. The molecular dynamics results are integrated into a direct-simulation Monte Carlo simulation and the simulated Rayleigh scattering intensities are compared with experimental data to test the models and direct-simulation Monte Carlo simulation results.

Nomenclature

b	=	impact parameter, m
$b_{i,m}$	=	cluster maximum impact parameter, m
b_m	=	maximum impact parameter, m
c_p	=	specific heat capacity, $J/(kg \cdot K)$
c_r	=	relative collision velocity, m/s
c_{ref}	=	reference relative collision velocity, m/s
d	=	diameter, m
d_c	=	cluster diameter, m
d_{ref}	=	reference diameter, m
d_0	=	molecule diameter, m
E	=	evaporation rate, s^{-1}
E_{int}	=	internal energy, J
E_L	=	latent heat, J
F_c	=	number of real particles per simulated particle
g	=	constraint force, N
$I'(II)$	=	Rayleigh scattering intensity
J	=	nucleation rate, s^{-1}
k	=	Boltzmann constant, J/K
L	=	specific latent heat, J/kg
M_i	=	cluster mass, kg
m	=	molecule mass, kg
n_c	=	number of new simulated particle
n_i	=	cluster number density, m^{-3}
n_o	=	reservoir number density, m^{-3}
P	=	probability
P^i_{av}	=	average sticking probability
q	=	charge, C
R	=	gas constant, $J/(kg \cdot K)$
r_c	=	cluster radius, m
r_i	=	cluster radius, m
r_*	=	critical cluster radius, m
$\mathbf{r}'$	=	intermediate bond vector before SHAKE algorithm
$\mathbf{r}^0$	=	original bond vector before Verlet algorithm
T	=	temperature, K
T_c	=	cluster temperature, K
$\mathbf{v}$	=	velocity, m/s
v_{rel}	=	relative velocity, m/s
α_i	=	cluster polarizability, $C \cdot m^2/V$
α_1	=	monomer polarizability, $C \cdot m^2/V$
Δt	=	time step, s
ΔV	=	cell volume, m^3
ϵ_0	=	permittivity of free space, $m^{-3} \cdot kg^{-1} \cdot s^4 \cdot A^2$
ϵ^{LJ}	=	well depth of Lennard–Jones potential energy, J
μ	=	reduced mass of the two atoms, kg
ρ_l	=	liquid density, kg/m^3
ρ_v	=	vapor density, kg/m^3
σ	=	surface tension, J/m^2 or collision cross section, m^2
σ^{LJ}	=	diameter of Lennard–Jones potential energy, m

Presented as Paper 1185 at the 46th AIAA Aerospace Sciences Meeting and Exhibit, Reno, Nevada, 7–10 January 2008; received 11 August 2008; revision received 13 January 2009; accepted for publication 16 January 2009.

*Graduate Student, Department of Aerospace Engineering. Student Member AIAA.
†Postdoctoral Fellow, Department of Aerospace Engineering. Member AIAA.
‡Professor, Department of Aerospace Engineering. Associate Fellow AIAA.
§Professor, Department of Chemistry.

I. Introduction

THE condensation phenomenon in free expansion plumes that has been observed during the past several decades has a number of important aerospace applications. For example, space-borne optical systems may be sensitive to optical contamination of their local environment by gases or condensate particles produced by the operation of attitude control system (ACS) jets. Condensation has been observed in both space and laboratory measurements. Strong visible and UV signals due to solar scattering from condensed ACS jet exhaust gases have been observed and analyzed and condensed argon clusters from the propellant are thought to be responsible for this phenomenon [1]. In the 1995–1996 time frame, the Astra-2 experiment flew a small cold argon thruster to study far-field plume phenomenology. The flow inside the nozzle, near vicinity, and far field of the plume was also numerically studied by Ivanov and Markelov [2]. A comparison of numerical predictions and experimental data of the angular distribution of the relative pressure in the far field of the plume showed that it is necessary to take into account the process of argon condensation both inside the nozzle and in the near vicinity.

A spectacular visible plume of the translunar injection burn of a Saturn IV B spacecraft during the Apollo 8 mission was photographed by the Smithsonian Astrophysical Observatory on Mt. Haleakela, Hawaii. Analysis of visible signals indicated that condensed exhaust plume water vapor was able to produce large solar scattering signals [3]. Under the assumption of steady-state homogeneous nucleation, Wu [3] computed the accumulation of condensate as a function of the streamline coordinate from the Oswatitsch integral with a nucleation rate taken from classical

nucleation theory (CNT) and semi-empirical estimates of the local flowfield conditions. Condensation was thus estimated to have occurred at about 45 m downstream of the nozzle exit. Kung et al. [4] calibrated and reduced the raw photographic data and used a semi-empirical version of condensation theory to predict ice particle condensation and size distribution. Their analysis indicated that 5–10% condensation, with particle sizes in the 70–100 Å range, would be necessary to explain the observed data.

With respect to laboratory measurements, Hagena and Obert [5] performed a series of expanding plume experiments on homogeneous condensation for different gases and measured the cluster beams from the core of the plume flowfield. They deduced a scaling law that suggested that specific combinations of source pressure, temperature, and nozzle geometry will result in cluster beams with the same mean cluster size. An Arnold Engineering Development Center (AEDC) program known as CONSET performed experiments to determine the onset and growth properties of condensate clusters in a typical exhaust plume flowfield and the dependence of the condensation process on nozzle geometry, reservoir conditions, molecular parameters, and flow species, such as argon, oxygen, and water. The laser-Rayleigh scattering technique was used to characterize the distribution and growth of clusters as well as condensation onset and scaling law experiments were performed for different species including water. Koppenwallner and Kankert [6] also studied condensation in free jet expansions from sonic orifices for different stagnation temperatures, pressures, and nozzle throat diameters with nitrogen, water vapor, and argon as test gases. Both pressure probe and laser light scattering were used to detect the condensation onset points on the centerline of all free jets and the results were compared with CNT theory.

Previous steady-state calculations, such as those mentioned previously, do not simulate the movement of clusters and collisions between clusters and monomers. To simulate microscopic nucleation, a kinetic approach, the direct-simulation Monte Carlo (DSMC) method, was recently developed and applied to homogeneous condensation in a free argon expansion rocket plume [7–10]. Based on the assumption that the cluster has bulk properties, the CNT method was used to define the cluster formation free energy. Assuming a maximum cluster size and a constant vapor number density, a nucleation rate at steady state was derived from the kinetic cluster evolution equations. To obtain the cluster–monomer and cluster–cluster collision models as well as the determination of cluster size, the molecular dynamics (MD) method was used to calculate the collision and sticking probabilities between clusters and monomers for an argon gas [10]. Homogeneous water condensation was simulated using the DSMC method for the Progress plume [11] using classical nucleation theory. Recent experimental research suggests that the water classical nucleation rate should be multiplied by a correction factor which is a function of the vapor temperature [12] and the corrected nucleation rate was found to have a great impact on the cluster-growth processes and flow macroparameters obtained in the DSMC simulations of the rocket exhaust plume [11].

The main goal of this paper is to improve the fidelity of the water condensation models used in DSMC simulations by rigorous MD methods. However, in contrast to argon, the simple polyatomic water system cannot be modeled as a Lennard–Jones gas and exhibits internal degrees of motion. MD studies of water condensation must incorporate both of these factors, and, in particular, there have not been many MD studies of the water cluster kinetics in the gas phase, except for the work of Schenter et al. [13]. In that work, a recent theory of water vapor-to-liquid phase nucleation was developed based on the kinetics of cluster formation and decomposition [13]. The new method used variational transition state theory to obtain the evaporation and condensation rate constants needed for a kinetic model of nucleation. Simulation of homogeneous condensation requires cluster–monomer collisions, cluster–monomer sticking processes, cluster evaporation, cluster–cluster collisions, and cluster nucleation models. In this work we apply our advanced MD studies to the first two of these processes and compare with the recent results of [13].

The outline of the remainder of the paper is as follows. In the following section we provide an overview of the DSMC method, particularly with respect to the condensation modeling. Reviews of the classical nucleation and evaporation models are also discussed. In Sec. III the simple point charge (SPC) water model is presented and the MD numerical techniques such as the Verlet algorithm, the SHAKE algorithm [14], and the Monte Carlo canonical ensemble procedure are reviewed. The implementation of these techniques provides MD-based cluster collision, and sticking probabilities are discussed in Sec. IV. Finally, the new MD and the classical nucleation and evaporation condensation models are used in the DSMC to simulate the laboratory Rayleigh scattering measurements of a water condensate flow.

II. Overview of DSMC Modeling of Condensation Coupled Flows

In the basic DSMC procedure, the entire flow volume is divided into cells and filled with simulation particles which represent real molecules and clusters. The cell size is defined by the local mean free path, and the number of the simulation particles representing a given species (molecular species or clusters) in the cell is defined as the ratio of the number of real particles to a preset F_{num} (the number of real particles represented by a simulated particle). Each simulated molecule is characterized by spatial coordinates, velocity, internal energy, and species-related mass. The simulated clusters are, in addition, characterized by the number of molecules they comprise.

The basic principle of DSMC is that the continuous process of particle movement and interaction is uncoupled. First, at each time step every particle is moved according to its velocity. Next, the interaction between the particles is modeled by appropriate coarse-grained models, for example, by collision models. Therefore, the DSMC time step should be chosen such that the particles move only a fraction of the cell size during the time step. Three types of interactions exist in the DSMC model: 1) molecule–molecule (M-M) collisions, 2) molecule–cluster (M-C) collisions, and 3) cluster–cluster (C-C) collisions.

The variable hard sphere (VHS) model is used to model simulated molecules representing real atoms or molecules in the plume, and the Larsen–Borgnakke model is used to redistribute molecule–molecule collision energy, based on the number of degrees of freedom. Cluster–cluster collisions that can result in coalescence are simulated by the semi-empirical Ashgriz–Poo model [15]. However, they were not found to be important for the conditions simulated in this work. The molecule–cluster collisions are modeled through the MD simulations of the water molecule system to be discussed in the next section.

In addition to the cluster–monomer interaction model, nucleation and evaporation are two key models in our DSMC simulation of condensation coupled flow. In the current work, we continue to use the CNT for these two models. We briefly review these models because they will be used in Sec. V to model condensation in a water free expanding plume. Detailed descriptions of these models can be found in [8].

Following CNT theory [16], initial clusters, called nuclei, are introduced into the computational domain. The nuclei have the same size as the local critical clusters, and they are in an equilibrium state with the surrounding gas. The nucleation rate J is given in the CNT theory as

$$J = \left(\frac{2\sigma}{\pi m^3}\right)^{\frac{1}{2}} \frac{\rho_v^2}{\rho_c} \exp\left(-\frac{4\pi r_*^2 \sigma}{3kT}\right) \tag{1}$$

where σ is the cluster surface tension, m is the molecular mass, ρ_v is the vapor density, ρ_c the cluster density, and r_* is the local critical cluster radius. Thus, during a time step Δt, in a cell with volume ΔV, the number of new simulated nuclei n_c is calculated as

$$n_c = J \Delta V \Delta t / F_c \tag{2}$$

where F_c is the number of real molecules represented by a simulated cluster molecule. The latent heat, generated during the nucleation

process, is evenly distributed to each number of degree of freedom of the ambient gas molecules in a cell. Using bulk theory, the latent heat, E_L, is given by

$$E_L = LM_i \tag{3}$$

where L is the specific latent heat, and M_i is the mass of a cluster consisting of i monomers. Because CNT assumes that the clusters have properties of the bulk material, we characterize the internal energy of a cluster in terms of the specific heat capacity of the bulk material, c_p, as

$$E_{\text{int}} = c_p M_i T_c \tag{4}$$

where i is the number of molecules in the cluster, T_c is the cluster temperature which initially is assumed to be the local gas translation temperature, and M_i is the cluster mass. The cluster evaporation rate, E, is given in the CNT theory as

$$E = \frac{4\pi p_s r_c^2}{(2\pi m k T_c)^{0.5}} \exp\left(\frac{2\sigma}{\rho R T_c r_c}\right) \tag{5}$$

where p_s is the vapor saturation pressure and R is the ideal vapor constant. In the evaporation process, the evaporated monomers gain translational and internal energy, reducing the internal energy of the original cluster. The details of the computational method of the nucleation and evaporation models are given in [7].

III. Molecular Dynamics Methodology of Water System

Molecular dynamics [17] is a form of computer simulation wherein atoms and molecules are allowed to interact for a period of time under known laws of physics, giving a view of the motion of the atoms. In this work, the outcomes of molecule–cluster collisions will be explored with MD simulation.

A. Simple Point Charge Water Model

The interactions among water molecules are dominated by dipole interactions. One effective way to describe such interactions is to consider three point charges, one on each atom. In the SPC model [18], the water molecule is modeled to have three centers of concentrated charge: a positive charge on each of the two H atoms and a negative charge on the O atom. The assumption that there are point charges is an approximation that leads to an incorrect value for the permanent dipole moment of the water molecule. To correct this, the H-O-H bond angle is changed from the true value of 104.45 to 109.47 deg in the SPC model. As a consequence of the charge concentration and the widened V-shaped bond angle, the permanent dipole moment of the SPC-model water molecule has a value close to that measured in experiment of 1.85 D.

In summary, the SPC model consists of a triangular water model with an OH distance of 1 Å (compared to the true bond length of 0.9584 Å), with point charges on the oxygen and hydrogen positions of -0.82 and $+0.41$ e (electronic charge units), respectively. The corresponding potential is a combination of Lennard–Jones interactions between the oxygen atoms of each water molecule,

$$U^{\text{LJ}}(r) = 4\epsilon^{\text{LJ}}\left[\left(\frac{\sigma^{\text{LJ}}}{r}\right)^{12} - \left(\frac{\sigma^{\text{LJ}}}{r}\right)^{6}\right] \tag{6}$$

with the parameters of $\sigma^{\text{LJ}} = 3.166$ Å, $\epsilon^{\text{LJ}} = 0.65$ kJ/mol, and the Coulomb potential between all the atoms,

$$U_{ij}^{\text{Coulomb}}(r_{ij}) = \frac{q_i q_j}{4\pi\epsilon_0 r_{ij}} \tag{7}$$

where q_i and q_j are the charges of the O or H atoms, and ϵ_0 is the permittivity of free space.

B. Integrating the Equations of Motion

In this work we choose the Verlet algorithm for the numerical integration of classical equations of motion because it is simple to implement and has a high-order accuracy,

$$\mathbf{r}(t + \Delta t) \approx 2\mathbf{r}(t) - \mathbf{r}(t - \Delta t) + \frac{\mathbf{f}(t)}{m}\Delta t^2 \tag{8}$$

where the estimation of the new position, $\mathbf{r}(t + \Delta t)$, is accurate to within $\mathbf{O}\Delta t^4$. The velocity can be derived from the particle trajectory as

$$\mathbf{v}(t) = \frac{\mathbf{r}(t + \Delta t) - \mathbf{r}(t - \Delta t)}{2\Delta t} + \mathbf{O}\Delta t^2 \tag{9}$$

where it may be seen that this expression for the velocity is accurate to order $\mathbf{O}\Delta t^2$.

C. SHAKE Algorithm

In addition to the interactions between water molecules as described by the SPC potential, intramolecular interactions need to be modeled. In the case of molecules such as water, one of the internal motions involves vibrations. However, vibrational motion is inherently quantum mechanical, especially for H atoms at the very low temperatures of interest to this study. If internal vibrations were included in the MD simulations, there would be an artificial exchange of energy between the collisions and the internal vibrational motion. Because this energy transfer is not allowed by quantum mechanics, we constrain the molecules to be rigid, thus no energy may be transferred to the vibrational motion. One method of constraining the bond lengths is the SHAKE algorithm. At each time step, a constraint force is added to the integrator to maintain a constant bond length

$$\mathbf{g}_{ij} \approx \frac{\mu_{ij}(r_{ij}^2 - r_{ij}'^2)}{2\Delta t^2 \mathbf{r}_{ij}^0 \cdot \mathbf{r}_{ij}'}\mathbf{r}_{ij}^0 \tag{10}$$

and enters into the Verlet algorithm, Eq. (8),

$$\mathbf{r}(t + \Delta t) = \mathbf{r}'(t + \Delta t) + \frac{\mathbf{g}(t)}{m}\Delta t^2 \tag{11}$$

where $\mathbf{r}'(t + \Delta t)$ is the position which would have been reached in the absence of any constraints.

For a system of simple diatomic molecules, computation of the constraint force would allow the correct atomic positions to be calculated in one pass. However, in the general polyatomic case this correction is merely an interim adjustment, not only because the above formula is approximate, but because the successive correction of the bonds in a molecule has the effect of perturbing the previously corrected bonds. The SHAKE algorithm therefore is iterative, with the correction cycle being repeated for all bonds until each has converged to the correct length, within a specified tolerance.

D. Monte Carlo Canonical Ensemble Simulation

For cluster–monomer interactions, the initial separations between molecules inside a cluster and the velocities of each molecules have a great effect on the collision–noncollision and sticking–nonsticking results. Therefore 100 initial configurations are chosen to eliminate the statistical error. To prepare the initial position configurations for clusters, the Monte Carlo canonical ensemble simulation method is used [13]. In this approach, a sphere domain is set up with a known radius, R_i, which depends on the cluster size, i. The initial molecules (for example, two molecules for a dimer) then are randomly put in the spherical domain and the system potential energy is calculated based on the SPC model and designated as U_o. The system is allowed to evolve for a large number of steps and for each time step, one of the molecules is randomly moved in the sphere and the new energy U_n is calculated. The move is accepted with probability,

$$P_a = \min(1, \exp(-[U_n - U_o))/kT) \tag{12}$$

where T is the temperature and k is Boltzmann's constant. After 10,000 steps, the system is assumed to be in equilibrium and one accepted configuration is recorded every 100 steps. The system is run until 100 configurations of molecule positions are obtained.

For each of the selected configurations, the Monte Carlo method does not tell us the velocities of the molecules inside a cluster, which are needed to perform the MD simulations. To determine these velocities the molecule's total energy is partitioned into translational and rotational energy (vibration is assumed to be negligible) and the two modes are assumed to be independent. For each molecule, the translational $\mathbf{v}_{\text{trn}}$ and rotational velocities $\mathbf{v}_{\text{rot}}$ are each randomly chosen. The corresponding translational, or rotational energy, E, is calculated and the velocity is accepted with probability, P_B, based on a Maxwell–Boltzmann distribution,

$$P_B(E) = 2\left(\frac{E}{\pi(kT)^3}\right)^{1/2} \exp\left(\frac{-E}{kT}\right) \tag{13}$$

where T is the cluster temperature. The molecule's velocity is then the sum of the translational and rotational velocities, that is, $\mathbf{v} = \mathbf{v}_{\text{trn}} + \mathbf{v}_{\text{rot}}$. At the end of the Monte Carlo ensemble initialization procedure, the molecules in the clusters have velocities and positions consistent with a system of 100 clusters in equilibrium at a temperature of T.

IV. Use of MD to Develop Cluster Collisions and Sticking Models

The cluster–monomer collision process may be used to define the cluster cross section, as the outcome of a monomer–monomer collision defines molecular cross section in traditional gas dynamics [10]. To characterize the cluster model, the collision processes of cluster monomers are simulated with the MD method, for various impact parameters b, cluster temperature T, and relative velocities v_{rel}. Sticking collisions are obviously counted as effective collisions, while for nonsticking collisions, only trajectories in which the deflection angle is at least 5 deg are counted as collisions.

The collision probability for each case (b, T, v_{rel}) is defined as the ratio of the number of trajectories that resulted in a collision to the total number of trajectories. For each case, a sample of 2500 trajectories is used with the orientation of the target cluster to the monomer randomly chosen. The colliding water molecule (monomer) is initially placed approximately 20 Å away from the cluster, a distance far apart such that the interaction between the cluster and the collider is sufficiently negligible.

The total simulation time for a case is approximately 30 ps, which is also long enough to observe whether the interaction outcome is a collision or noncollision interaction because it takes about 10 ps before the atom is in the vicinity of the target cluster. The impact parameter b increases from a head-on collision value of zero to a value in which the cluster–monomer collision probability is close to zero. Relative collision velocities from approximately 193 to 473 m/s are chosen, the cluster temperature ranges from 40 to 243 K, and the cluster sizes selected for study in the MD simulations ranges from a dimer up to 500-mers. The ranges of cluster size, relative collision velocity, and cluster temperature are typical of those found in a condensation plume flow.

A. Cluster Radius

Figure 1 shows a comparison of the MD simulation results of collision probabilities for cluster–monomer collisions with a relative collision velocity of 360 m/s and cluster temperature of 140 K. The collision probability is close to unity for the collisions with relatively small impact parameters. It can be seen that for different cluster sizes, there is a critical impact parameter b_s, below which the probability is close to unity and for impact parameter greater than b_s, the probability decreases rapidly to zero.

The maximum impact parameter b_m, chosen here to correspond to a collision probability of 0.1, can be used to calculate the cluster–monomer collision cross section, σ, as $\sigma = \pi b_m^2$. It may be related to the cluster and monomer diameters by [19]

$$b_m = \frac{d_c + d_0}{2} \tag{14}$$

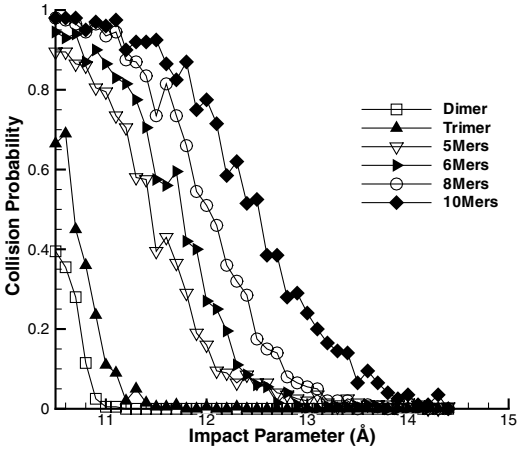

Fig. 1 Collision probabilities for cluster–monomer collisions with a relative collision velocity of 360 m/s and cluster temperature of 140 K.

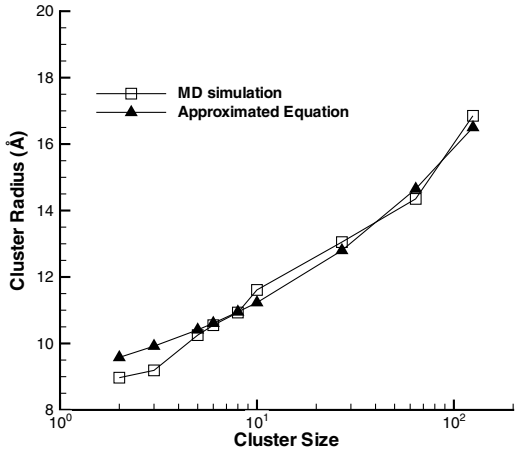

Fig. 2 Average cluster radius with a relative collision velocity of 360 m/s and cluster temperature of 140 K.

Thus, the cluster radius, $r_i = d_c/2$, can be determined from the MD simulation results, because the monomer diameter is known.

Figure 2 shows the corresponding radii r_i, for different cluster sizes i, and that the MD results may be fitted to an analytical general cluster-radius equations [20]:

$$r_i = Ai^{\frac{1}{3}} + B \tag{15}$$

where the values obtained from the fit are $A = 1.85$ Å and $B = 7.25$ Å. Because water is a polyatomic system its clusters are larger than those of argon wherein values of $A = 2.3$ Å and $B = 3.4$ Å were previously obtained [10].

B. Variable Hard Sphere Model for Cluster–Monomer Collisions

Cluster–monomer collision probabilities may also be a function of the relative collision velocities. Results of collision probabilities for different cluster sizes (dimers and 8-mers) and relative collision velocities are shown in Fig. 3. Each symbol represents an average of 2500 trajectory results. It can be seen that the critical impact parameter increases as the relative velocity decreases. As the velocity decreases, the time the monomer resides in the vicinity of the cluster increases. The monomer therefore receives a greater impulse increasing its chance to change its velocity which, in turn, increases the critical impact parameter. Because the dimers are small in size, the collision probability is sensitive to the dimer cluster orientations. This sensitivity causes the collision probability curves for the dimers to appear to be noisier than the 8-mer case. To model the dependence

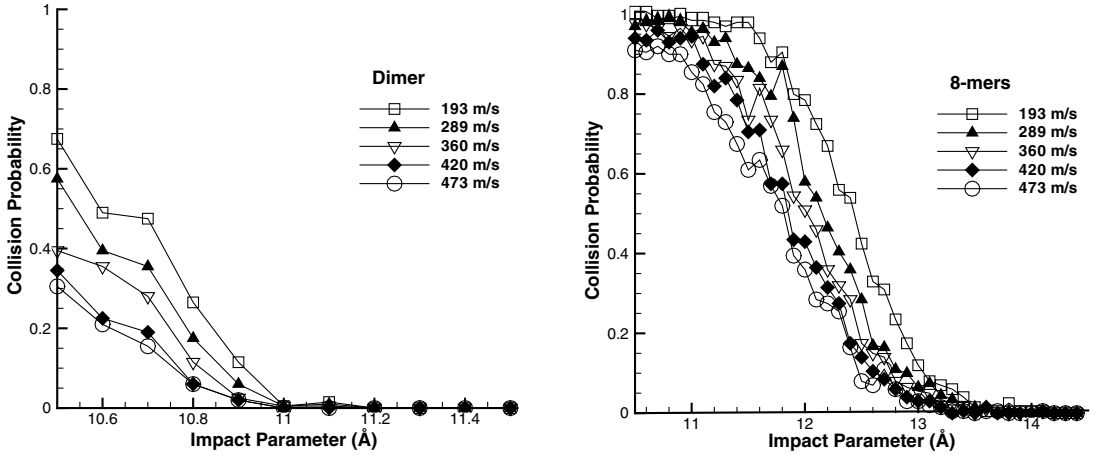

a) Dimer **b) 8-mers**

Fig. 3 Comparison of collision probability for two cluster sizes at 140 K and different relative velocities.

of cluster diameter on the relative collision velocity c_r, we use the VHS [19] model which is stated in the following relationship:

$$d = d_{\text{ref}} \left(\frac{c_{\text{ref}}}{c_r} \right)^{\nu} \tag{16}$$

where the subscript "ref" refers to a reference value and ν is a constant related to the species viscosity. The cluster-radius values obtained from the MD simulations (symbols) are shown as a function of relative collision velocity for different cluster sizes at a cluster temperature of 140 K in Fig. 4. For each cluster size case we use the reference diameter, d_{ref}, shown in Fig. 2 for a reference velocity, c_{ref} of 360 m/s. Then the value of ν is varied until a smooth fit through all the pairs of velocities and diameters is obtained. Figure 4 shows that ν ranges from 0.07 to 0.1 which is relatively small compared to the value for water monomers of 0.25. Since ν for water clusters is close to zero, the VHS model reduces to a hard sphere model, that is, the cluster radius is independent of collision relative velocities.

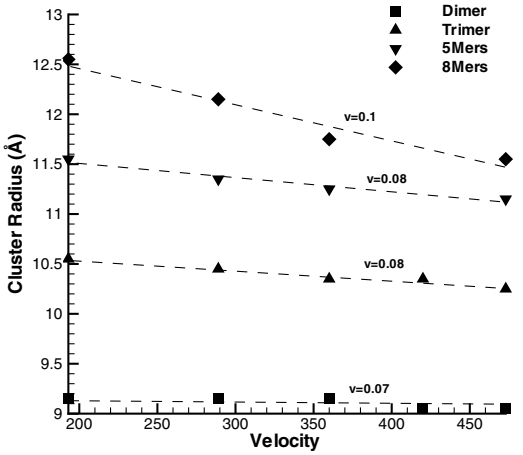

Fig. 4 Cluster radii shown as symbols from MD are fitted to VHS model by choosing the constant ν.

Cluster–monomer collision probabilities may also be a function of the cluster temperature. Collision probabilities for different cluster sizes (dimers and 8-mers) and cluster temperature are shown in Fig. 5. It can be seen that the critical impact parameter increases as the cluster temperature and size increases. Figure 6 shows the cluster radius for different cluster temperatures at a cluster collision relative velocity of 360 m/s. Because the maximum variation is 8% (for 5-mers), similar to previous work on argon [10], we will assume that cluster radius also does not depend on temperature and a hard sphere model will be used in DSMC calculations.

C. Sticking Collision Probability

The sticking probability for a collision process between a cluster and a molecule can be simulated in a manner similar to the collision probability. Initially, the target water cluster is at the origin with a center of mass velocity at zero, but it has internal rotational motion. The colliding water molecule (monomer) is initially placed approximately 20 Å away from the cluster. The total simulation time

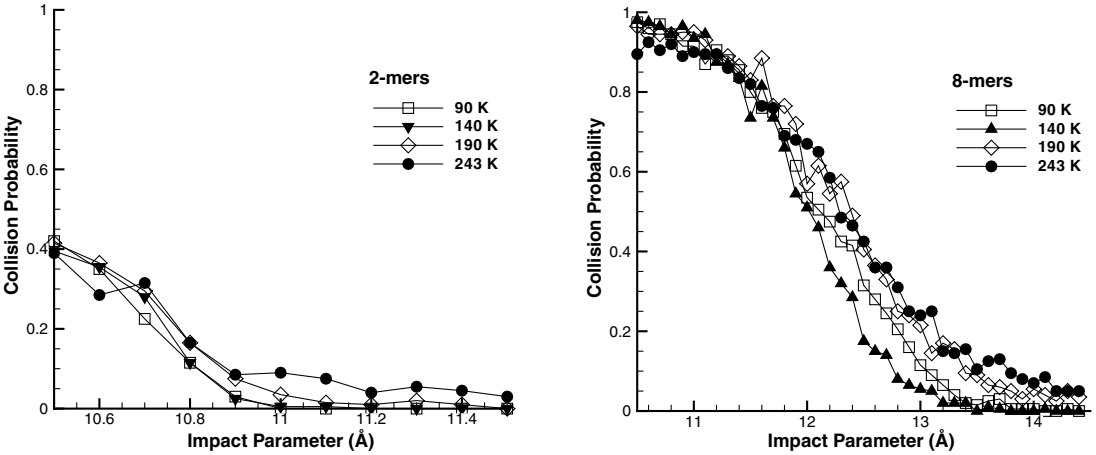

a) Dimer **b) 8-mers**

Fig. 5 Comparison of collision probability for a collision velocity at 360 m/s and different cluster temperatures.

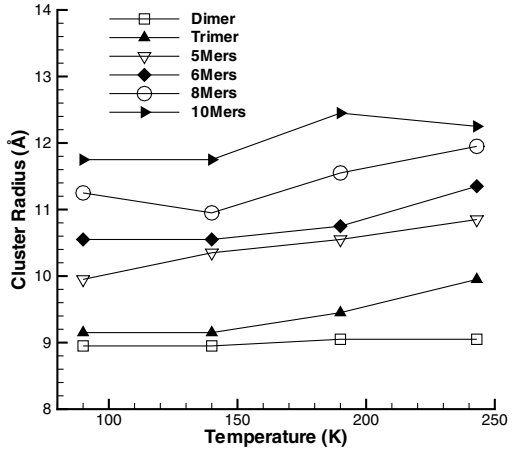

Fig. 6 Cluster radius shown as symbols from MD simulations for different cluster temperatures at a cluster collision relative velocity of 360 m/s.

for a colliding case is approximately 30 ps, which is also long enough to observe whether the collision outcome is a sticking or nonsticking collision because it takes about 10 ps before the atom collides with the target cluster. To obtain good statistics, we perform 2500 trajectories for each colliding case by randomly rotating the target cluster and water molecule.

In the DSMC simulation of an expanding flow, consisting of gas and clusters, each collision is not modeled in detail and only average collision properties are used. For this reason, the dependence of the sticking probability on impact parameter must be averaged over the collision cross section. The average sticking probability P^i_{av} can be calculated from the MD results for each cluster based on a b^2 distribution of collision pairs,

$$P^i_{\text{av}} = \frac{1}{b^2_{i,m}} \int_0^{b_{i,m}} P(b) \mathrm{d}b^2 \tag{17}$$

where $b_{i,m}$ is the cluster maximum impact parameter or collision radius for a cluster of size i.

It can be expected that the cluster–monomer sticking probability is also dependent on the relative collision velocity, especially for small clusters. Similarly to the collision probability, Fig. 7 shows that the sticking probability decreases as the relative velocity increases and cluster size decreases. The sensitivity of the sticking probability to relative velocity decreases as the cluster size increases, and it may be neglected for the clusters larger than 10-mers with good approximation. For the collision velocity range of 193 to 473 m/s, we may neglect the velocity effects on the sticking probability in the DSMC calculations.

Figure 7 shows that sticking probability is also dependent on cluster temperature, especially for small clusters. Figure 8 shows that the sticking probability decreases as the cluster temperature increases. The sensitivity of the sticking probability to relative

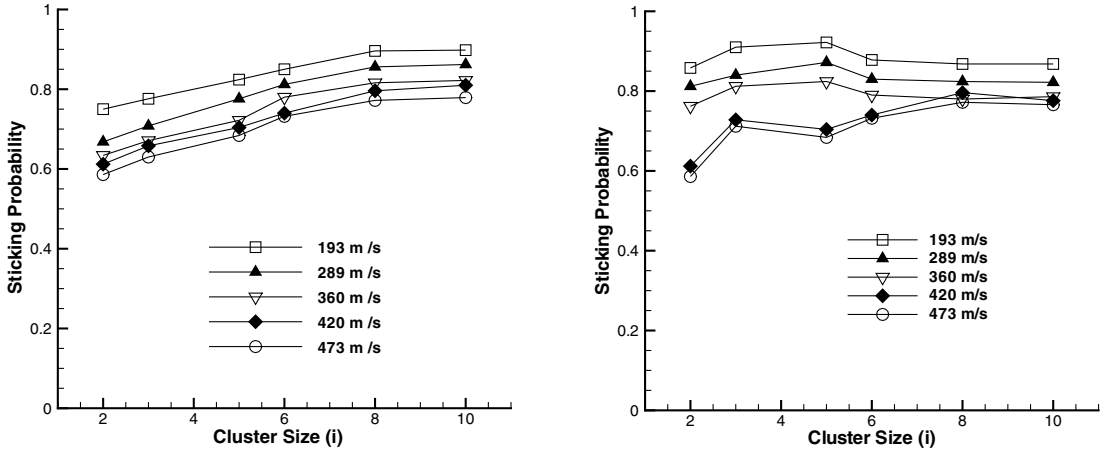

a) 140K **b) 90K**

Fig. 7 Comparison of sticking probability for two different temperatures.

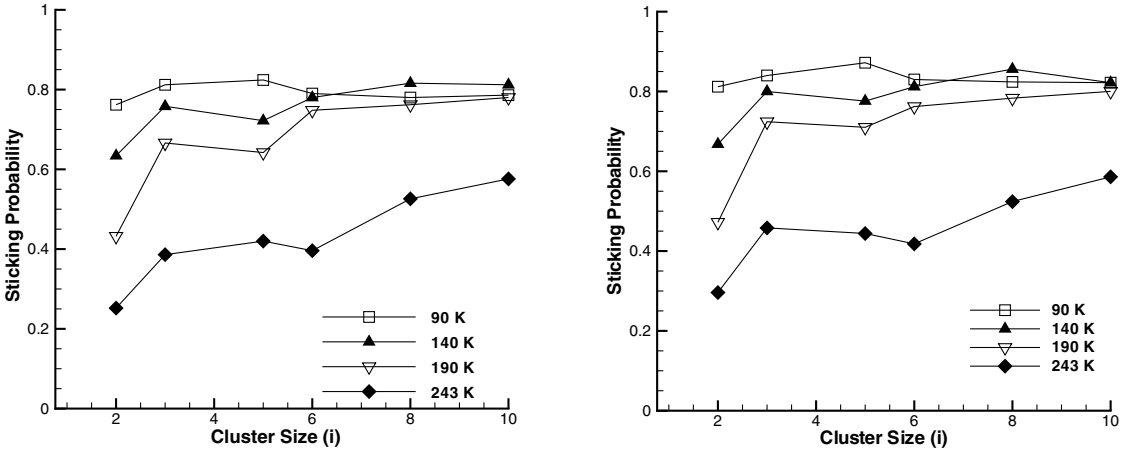

a) 360 m/s **b) 289 m/s**

Fig. 8 Comparison of sticking probability for two different collision relative velocities.

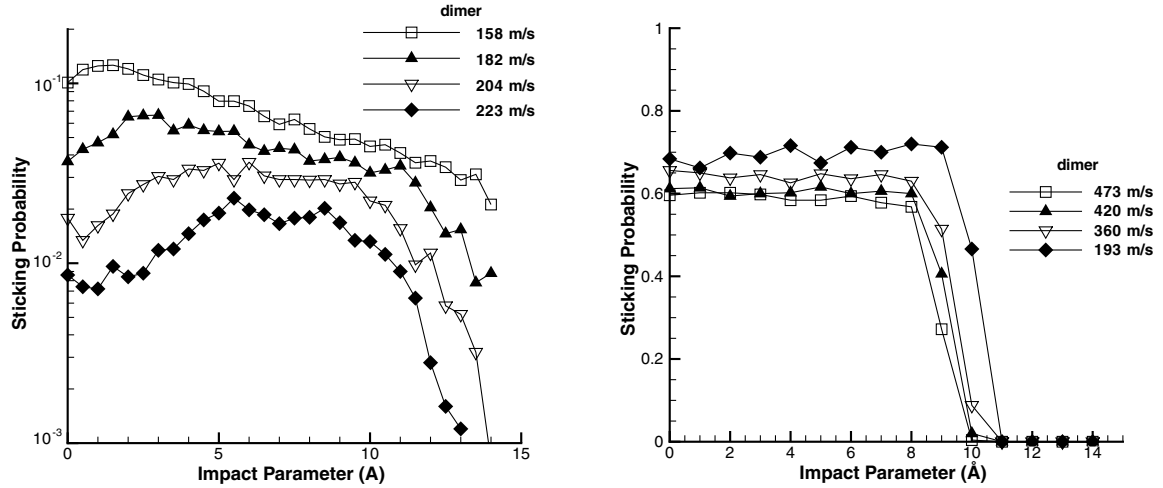

a) Argon b) Water

Fig. 9 Comparison of sticking probability for two different systems. Both cases have a temperature of 140 K.

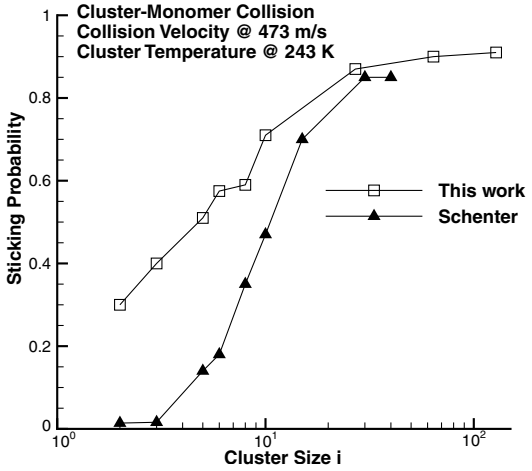

Fig. 10 Comparison of sticking probability for water cluster–monomer collisions with the results of Schenter et al. [13]. Both cases are at a temperature of 243 K and an impact parameter at zero.

velocity decreases as the cluster size increases, and it may be neglected for the clusters larger than 10-mers with good approximation. It is also seen that at 243 K, the sticking probability is relatively low compared to other temperatures. These results indicate that unlike our previous argon condensation simulations [10], we must consider the temperature effect on the sticking probabilities in the DSMC simulations.

Figure 9 shows the comparison of sticking probabilities for argon and water dimer–monomer collision simulations at a temperature of 140 K. The water sticking probability is significantly higher than the argon cases because the water potential well depth is about 20 times larger than that of argon. Therefore higher water condensation rates are expected in the subsequent DSMC calculations.

Figure 10 shows a comparison of sticking probabilities for water dimer–monomer collision simulations with the work [13] of Schenter et al., the only published water MD results of sticking probabilities in the gas phase. Both simulations predict that the cluster–monomer sticking probability increases as the cluster size increases. For cluster sizes less than 10, our sticking probability is larger than that of Schenter et al. [13]. This is probably because the potential well depth used in this work is larger than the value used in [13]. The potential used in [13] is that of Dang and Chang [21], also considered an accurate potential for modeling interactions between water molecules. The difference in the sticking probability results provides quantification of the sensitivity of the MD results to the selection of water potential.

The figure also shows that for cluster size less than 10, the sticking probability increases quickly as the cluster size increases, however, for cluster size as larger than 10, the sticking probability slowly approaches unity. In summary, the MD simulation results show that cluster–monomer collisions may be modeled with the hard sphere model and with a sticking probability that depends on cluster temperature as given in Fig. 8.

V. DSMC Simulations of Condensation Plumes

The condensation models discussed in the preceding sections are now applied to two expanding condensation plumes experimentally studied in the Arnold Engineering Development Center (AEDC) [22]. A conical nozzle with a throat diameter of 1.0 mm, a nozzle length of 5.334 mm, and an angle of 10.5 deg is attached to a research chamber with stagnation pressures and stagnation temperatures listed as cases 1a and 2a in Table 1. The water vapor inside the chamber expands through the nozzle into a vacuum environment and condensation occurs outside the nozzle. Cases 1b and 2b use an artificially increased nucleation rate of 50 greater than the one given by CNT and the results of these simulations will be discussed in Sec. V.E. The influence of the cluster size and temperature on the sticking coefficients is investigated and discussed in Sec. V.C by considering a case, where a sticking probability of unity is assumed, case 1c.

The problem under consideration is complicated by the large variation in number density from the nozzle throat to the plume far field. The Knudsen number, defined as the ratio of the mean free path to the characteristic length (the nozzle throat), is on the order of 10^{-3} at the nozzle throat. This indicates that a computation cell length of 10^{-6} m is required and based on the speed of the flow (500 m/s at the throat), a time step on the order of 10^{-9} is necessary. Because the flow is expanding, however, such small cell sizes and time steps may not be necessary for most of the computational domain.

To reduce the computational cost, two DSMC calculations, one from the nozzle throat to a small region beyond the nozzle exit

Table 1 Computational cases in this work

Case no.	P_0, atm	T_0, K	Nucleation rate ratio	Sticking prob.
1a	0.08	386	1	MD
1b	0.08	386	50	MD
1c	0.08	386	1	Unity
2a	0.20	394	1	MD
2b	0.20	394	50	MD

Table 2 Computation parameters in DSMC calculations

Calculations	Inside and near nozzle	Far field
Time step, s	2×10^{-9}	2×10^{-8}
F_{num}	5×10^{9}	5×10^{9}
Domain size, m^2	0.01×0.004	0.1×0.04
No. cells	100×40	100×40
Subcells per cell, up to	100×100	100×100
No. subcells	1.0×10^{6}	1.1×10^{6}
No. simulated particles	1.1×10^{6}	1.3×10^{6}

and the second in the far field, are performed. The original 2-D axisymmetric SMILE code [23] is modified to simulate nucleation, cluster–molecule and cluster–cluster collisions, and evaporation processes. The computational parameters for case 1a are listed in Table 2. Further information about these parameters can be found in [23].

A. Flow Inside and in the Vicinity of the Nozzle

The flow inside the nozzle is calculated as noncondensation flow and the gas-surface interaction at the nozzle wall is assumed to be fully accommodated at a temperature of 300 K. About 5 million simulated particles and 1.5 million subcells are used at the steady state and the results are sampled up to 100,000 time steps. The simulation takes about 80 h of computational time with 32 Intel Intel Xeon Processors of 3.06 GHz. The flow structure is shown in Fig. 11, in which density and Mach number contours of case 1a are plotted, respectively. The density drops by 2 orders of magnitude from the throat through the nozzle exit (assumed to be at a vacuum condition) and the typical growth of the boundary layer in the vicinity of the nozzle wall may be seen in Fig. 11.

We analyze the solution shown in the number density contours in Fig. 11 to find the density contour corresponding to $Kn = 0.015$, a value where DSMC calculations are practical. We then construct a starting surface that corresponds to a number density of 7×10^{23} to begin the far-field calculation.

B. Far-Field Condensation Flow

Using the starting surface from the above calculation, for case 1a, we expand our computational domain 10 times in both axial and radial directions and a weighting factor of 10^{-5} for water clusters is used for better species resolution. About 1.3 million simulated particles and 1.1 million subcells are used at the steady state. Once the condensation is turned on, approximately, the calculation slowed down by a factor of 2 due to all the processes related to condensation. After the condensation coupled flow has reached steady state, the results are sampled up to 800,000 time steps. The simulation takes about 70 h of computational time with 32 Intel Intel Xeon Processors of 3.06 GHz.

Figure 12 shows the gaseous water vapor number density and gas and cluster temperatures along the plume centerline. The water vapor undergoes a free expansion and the number density drops by 2 orders of magnitude. The temperature decreases rapidly from 200 to 20 K. Because of the latent heat and nonequilibrium, the cluster temperature is always higher than the surrounding vapor molecules.

As discussed in our previous conference paper [24], initial cluster or nuclei appear in a nucleation region (close to the nozzle exit) where the cluster number density increases quickly along the flow direction. Upstream of this region, the gas is essentially an expanding plume without condensation. As shown in Fig. 13, farther downstream of the nucleation region, the cluster number density decreases, mainly due to the expansion. Because the cluster number density is only on the order of $10^{17}/m^3$, about 6 orders of magnitude less than the vapor number density, the condensation does not effect the gaseous flow. The average cluster size is typically below 10-mers in the nucleation region, whereas it increases downstream of the nucleation region to about 700 due to the sticking collision process between cluster and vapor molecules. It then slowly decreases after $X = 6D_0$ which indicates that the cluster evaporation process

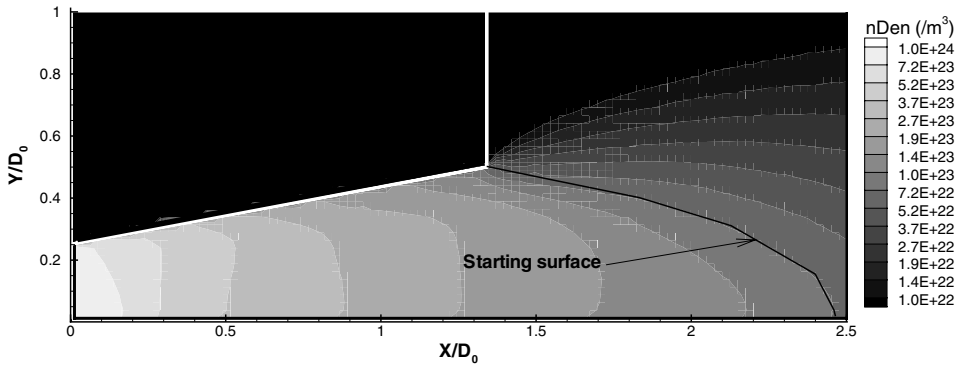

a) Number density contour

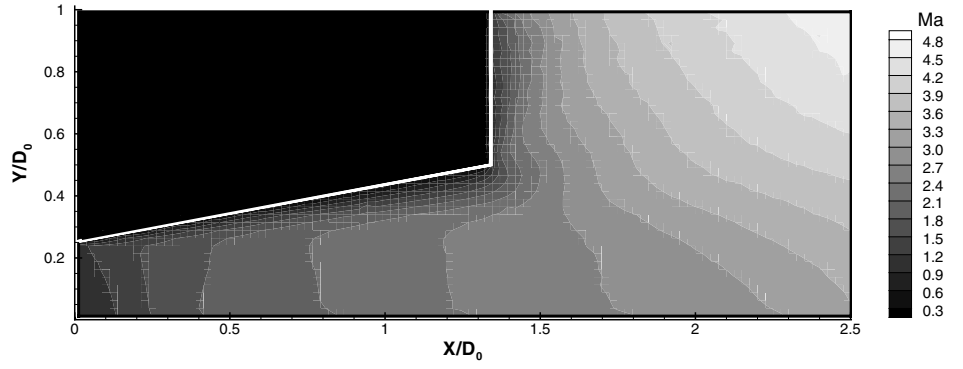

b) Mach number contour

Fig. 11 Number density and Mach number contours inside and near the nozzle (case 1a). Here D_0 is the nozzle exit diameter.

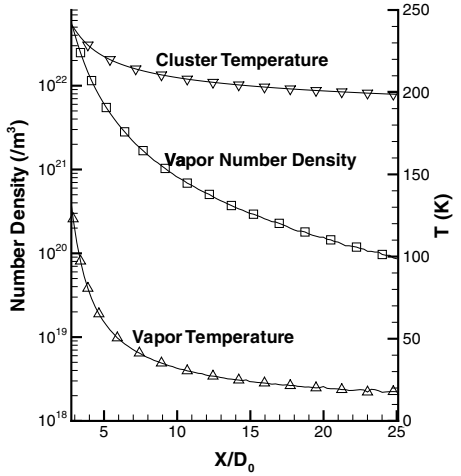

Fig. 12 Water vapor number density and gas and cluster temperatures along the plume centerline (case 1a). Here the X axis starts with the condensation onset which is about $2.8D_0$.

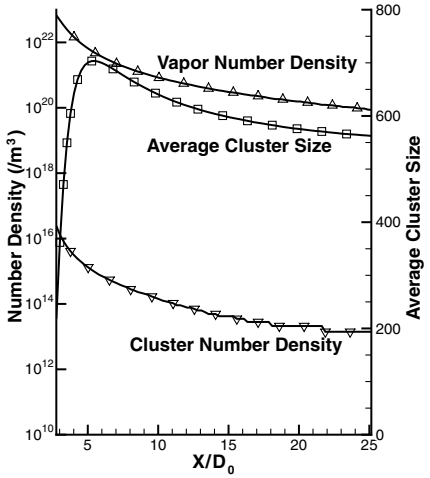

Fig. 13 Water vapor number density, cluster number density, and average cluster size along the plume centerline (case 1a).

becomes more important than that of cluster growth caused by sticking collisions.

C. Sensitivity of Results to Sticking Probability

To test the importance of using a sticking coefficient that is a function of the cluster temperature and size, the DSMC simulations are repeated in case 1c for the same nozzle stagnation conditions but with a constant sticking probability of unity. Figure 14 shows the comparison of cluster number density and average cluster size along the plume centerline for cases 1a and 1c. The cluster number density in case 1c is slightly higher than 1a but the cluster size in case 1c (for the sticking probability of unity) is significantly higher than the more accurate model (case 1a).

D. Comparison of Chamber Pressure Effect

The stagnation pressure of case 2a is about 2.5 times that of case 1a and the temperature of both cases is quite close. According to the classical nucleation theory, stronger condensation should be observed in case 2a. Figure 15 shows a comparison of water vapor and cluster number density and average cluster size along the plume centerline for cases 1a and 2a. It can be seen that the water vapor number density in case 2a is about 2 times that of case 1a but the average cluster size is about 5000 while in case 1a it is 700. The cluster number density in case 2a is slightly smaller than case 1a which is due to the fact that the average cluster size is 7 times larger although the reservoir pressure is 2.5 times higher than for case 1a.

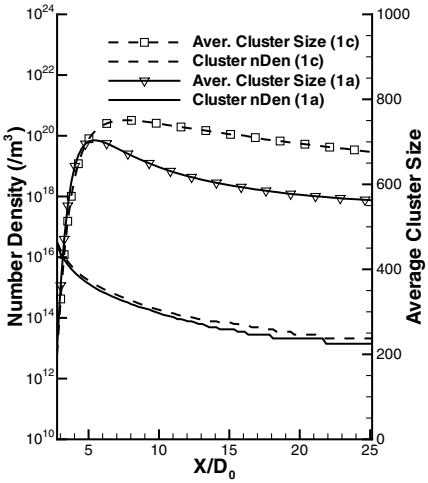

Fig. 14 Comparison of cluster number density and average cluster size along the plume centerline for cases 1a and 1c.

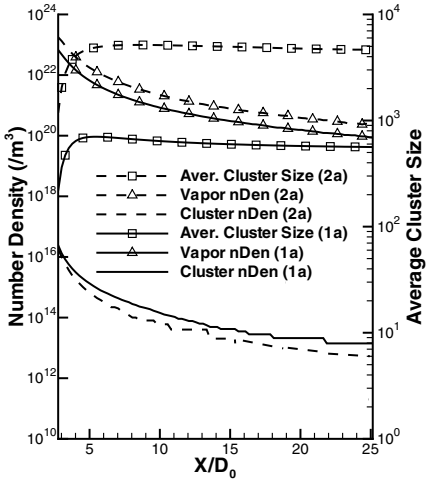

Fig. 15 Comparison of water vapor number density, cluster number density, and average cluster size along the plume centerline for cases 1a and 2a.

E. Comparison of Rayleigh Scattering Intensity

Assuming the condensing flowfield to be composed of a collection of gas phase monomers and molecular clusters, or i-mers, the single Rayleigh scattering intensity with polarization vector parallel to the incident beam's plane of polarization is

$$I'(II) = \sum_{i=1}^{\infty} \left(\frac{n_i}{n_o}\right)\left(\frac{\alpha_i}{\alpha_1}\right)^2 \tag{18}$$

where n_o is the reservoir number density of the flowfield [22]. The polarizability of a cluster of size i, α_i, is assumed to be i times of molecular polarizability α_1. The total intensity can be further divided into two parts,

$$I'(II) = \left(\frac{n_1}{n_o}\right) + \sum_{i=2}^{\infty} \left(\frac{n_i}{n_o}\right)\left(\frac{\alpha_i}{\alpha_1}\right)^2 \tag{19}$$

where the first and second terms on the right-hand side are the contributions to the intensity from the vapor intensity and clusters, respectively.

Figures 16 and 17 show the comparison of Rayleigh scattering intensity (solid line) calculated by Eq. (18) and AEDC data (open squares) of [22]. The contribution of the intensity due to clusters increases before $X = 0.015$ m, as the cluster size increases. After that, the cluster contribution to the intensity decreases as the cluster

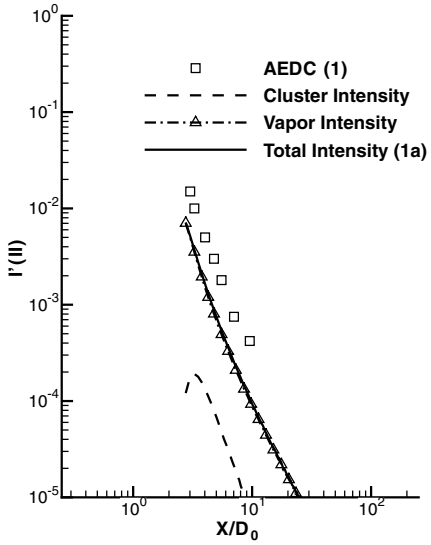

Fig. 16 Comparison of Rayleigh scattering intensity between AEDC data and case 1a simulation results.

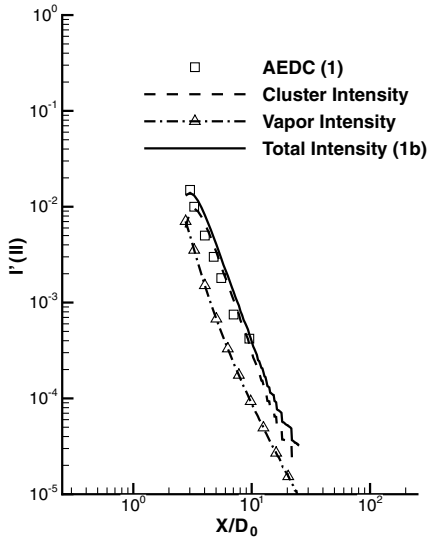

Fig. 18 Comparison of Rayleigh scattering intensity between AEDC data and case 1b (with 50 times CNT nucleation rate) simulation results.

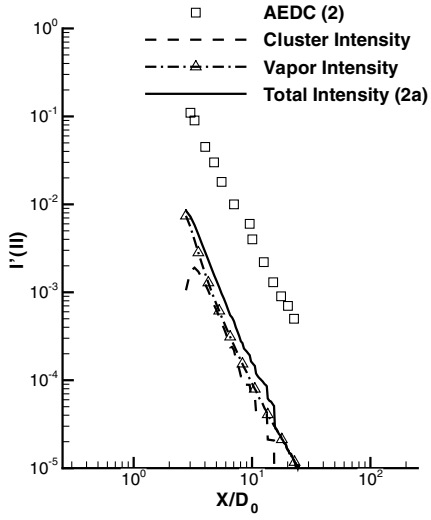

Fig. 17 Comparison of Rayleigh scattering intensity between AEDC data and case 2a simulation results.

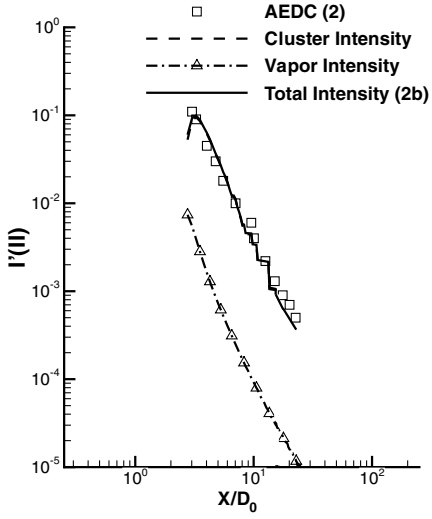

Fig. 19 Comparison of Rayleigh scattering intensity between AEDC data and case 2b (with 50 times CNT nucleation rate) simulation results.

size remains the same and the cluster number density decreases. In Fig. 16, the vapor intensity (triangles) overlaps with the Rayleigh scattering intensity and the cluster intensity is predicted to be only 3% of the vapor intensity. In Fig. 17, the higher stagnation pressure case, the vapor intensity remains the main contribution to the Rayleigh scattering intensity and similar to case 1a, the cluster intensity is about 2 orders of magnitude less than the AEDC measurement. In case 2a the cluster intensity (dashed line) is increased to 20% of the vapor intensity due to the stronger condensation, as discussed in Sec. V.D. For the two AEDC cases [22], the degree of condensation, defined as the ratio of the cluster mass to the total mass, is lower than 0.1% so that the vapor number density or vapor intensity is almost constant. Therefore, the difference between the total intensity and AEDC data may be reduced by increasing the cluster intensity which depends on the nucleation rate.

Zhong et al. [11] suggests that the water nucleation rate needs to be corrected by a factor of 10 to 0.1 for a vapor temperature of 220 to 260 K. In this work, we increase the nucleation rate by a factor of 50 for both stagnation pressures, designated as cases 1b and 2b and the results are presented in Figs. 18 and 19, respectively. In both cases the contribution to the total intensity due to the clusters is increased by a factor of about 50, making the cluster intensity the main contribution to the Rayleigh scattering intensity, especially in case 2b. The predicted Rayleigh scattering intensity obtained with the higher nucleation rate gives better agreement with both AEDC data cases. This correction, however, is ad hoc and in future work, a more fundamental kinetic nucleation model will be obtained from our improved MD simulations.

VI. Conclusions

In this work, accurate MD calculations were performed with the SPC water potential to develop condensation models of water monomer collisions and sticking probabilities to be used in DSMC simulations. Clusters size, cluster–monomer collision, and sticking probability calculations were performed to verify that for the temperature and velocity ranges in a typical free expanding plume the water clusters may be modeled with the hard sphere model and with a sticking probability that depends on cluster temperature. Comparison of water sticking probabilities with previous argon simulation results and an independent work was provided.

The MD simulation results were integrated into DSMC simulation of homogeneous condensation in a free expansion water plume through a conical nozzle. Rayleigh scattering intensities were calculated and compared with experimental data, indicating that our condensation model agrees reasonably well with the experimental data if the CNT nucleation rate is increased by a factor of 50.

Accurate water nucleation and evaporation models remain the key components of the DSMC condensation model which will be explored in future work.

Acknowledgments

The research performed at the Pennsylvania State University was supported by the U.S. Air Force Office of Scientific Research Grant No. F49620-02-1-0104 whose support is gratefully acknowledged. Special thanks to M. Ivanov of the Institute of Theoretical and Applied Mechanics, Russia for the use of the original SMILE code.

References

[1] Kolb, C. E., Lyons, R. B., Elgin, J. B., Huffman, R. E., Paulsen, D. E., and McIntyre, A., "Scattered Visible and Ultraviolet Solar Radiation from Condensed Attitude Control Jet Plumes," *Journal of Spacecraft and Rockets*, Vol. 20, No. 4, 1983, pp. 383–389. doi:10.2514/3.25611

[2] Ivanov, M. S., and Markelov, G. N., "Free-Flight Experiment and Numerical Simulation for Cold Thruster Plume," *Journal of Propulsion and Power*, Vol. 15, No. 3, 1999, pp. 417–423. doi:10.2514/2.5460

[3] Wu, B. J. C., "Possible Water Vapor Condensation in Rocket Exhaust Plumes," *AIAA Journal*, Vol. 13, No. 6, 1975, pp. 797–802. doi:10.2514/3.60440

[4] Kung, R. T. V., Cianciolo, L., and Myer, J. A., "Solar Scattering from Condensation in Apollo Translunar Injection Plume," *AIAA Journal*, Vol. 13, No. 4, 1975, pp. 432–437. doi:10.2514/3.49725

[5] Hagena, O. F., and Obert, W., "Cluster Formation in Expanding Supersonic Jets: Effect of Pressure, Temperature, Nozzle Size, and Test Gas," *Journal of Chemical Physics*, Vol. 56, No. 5, 1972, pp. 1793–1802. doi:10.1063/1.1677455

[6] Koppenwallner, G., and Dankert, C., "Homogeneous Condensation in Nitrogen, Argon and Water Free Jets," *Journal of Physical Chemistry*, Vol. 91, No. 10, 1987, pp. 2482–2486. doi:10.1021/j100294a008

[7] Zhong, J., "The Modeling of Homogeneous Condensation in Free-Expanding Plumes with the Direct Simulation Monte Carlo Method," Ph.D. Thesis, The Pennsylvania State University, University Park, PA, May 2005.

[8] Zhong, J., Zeifman, M., Levin, D., and Gimelshein, S., "Modeling of Homogeneous Condensation in Supersonic Plumes with the DSMC Method," *AIAA Journal*, Vol. 43, No. 8, 2005, pp. 1784–1796. doi:10.2514/1.9566

[9] Zhong, J., and Levin, D. A., "Development of a Kinetic Nucleation Model for a Free-Expanding Argon Condensation Flow," *AIAA Journal*, Vol. 45, No. 4, 2007, pp. 902–911. doi:10.2514/1.28234

[10] Zhong, J., Zeifman, M. I., and Levin, D. A., "Kinetic Model of Condensation in a Free Argon Expanding Jet," *Journal of Thermophysics and Heat Transfer*, Vol. 20, No. 1, 2006, pp. 41–51. doi:10.2514/1.15868

[11] Zhong, J., Zeifman, M. I., and Levin, D. A., "Sensitivity of Water Condensation in a Supersonic Plume to the Nucleation Rate," *Journal of Thermophysics and Heat Transfer*, Vol. 20, No. 3, 2006, pp. 517–523. doi:10.2514/1.18477

[12] Wolk, J., Strey, R., Heath, C. H., and Wyslouzil, B. E., "Empirical Function for Homogeneous Water Nucleation Rates," *Journal of Chemical Physics*, Vol. 117, No. 10, 2002, pp. 4954–4960. doi:10.1063/1.1498465

[13] Schenter, G. K., Kathmann, S. M., and Garrett, B. C., "Dynamical Benchmarks of the Nucleation Kinetics of Water," *Journal of Chemical Physics*, Vol. 116, No. 10, 2002, pp. 4275–4280. doi:10.1063/1.1448487

[14] Ryckaert, J. P., Ciccotti, G., and Berendsen, H. J. C., "Numerical-Integration of Cartesian Equations of Motion of a System with Constraints—Molecular-Dynamics of n-Alkanes," *Journal of Computational Physics*, Vol. 23, No. 3, 1977, pp. 327–341. doi:10.1016/0021-9991(77)90098-5

[15] Ashgriz, N., and Poo, J. Y., "Coalescence and Separation in Binary Collisions of Liquid Drops," *Journal of Fluid Mechanics*, Vol. 221, No. 1, 1990, pp. 183–204. doi:10.1017/S0022112090003536

[16] Abraham, F. F., *Homogeneous Nucleation Theory*, Academic Press, New York, 1974.

[17] Frenkel, D., and Smit, B., *Understanding Molecular Simulation: From Algorithms to Applications*, Academic Press, New York, 2002.

[18] Berendsen, H. J. C., Postma, J. P. M., van Gunsteren, W. F., and Hermans, J., "Interaction Models for Water in Relation to Protein Hydration," *Intermolecular Forces*, edited by B. Pullman, D. Reidel Publishing Co., Dordrecht, The Netherlands, 1981, pp. 331–342.

[19] Bird, G. A., *Molecular Gas Dynamics and the Direct Simulation of Gas Flows*, Clarendon Press, Oxford, England, U.K., 1994.

[20] Muller, H., Fritsche, H. G., and Skala, L., "Analytic Cluster Models and Interpolation Formulae for Cluster Properties," *Clusters of Atoms and Molecules 1: Theory, Experiment, and Clusters of Atoms*, edited by H. Haberland, Springer–Verlag, Berlin, 1995, pp. 115–138.

[21] Dang, L. X., and Chang, T., "Molecular Dynamics Study of Water Clusters, Liquid, and Liquid-Vapor Interface of Water with Many-Body Potentials," *Journal of Chemical Physics*, Vol. 106, No. 19, 1997, pp. 8149–8159. doi:10.1063/1.473820

[22] Lewis, J. W. L., and Williams, W. D., "Summary Report for the CONSET Program at AEDC," Aedc-tr-80-16, 1980.

[23] Ivanov, M. S., Markelov, G. N., and Gimelshein, S. F., "Statistical Simulation of Reactive Rarefied Flows: Numerical Approach and Applications," AIAA Paper 98-2669, June 1998.

[24] Li, Z., Zhong, J., Levin, D. A., and Garrison, B. J., "Modeling of Water Vapor Condensation in Expanding Plumes," AIAA Paper 2008-1185, 2008.

C. Kaplan
Associate Editor